Domains and domain walls in thin permalloy films

Stage verslag

Y. de Boer
Faculteit der Wiskunde en Natuurwetenschappen

Leiden, August 31, 2005

The work described in this document has been done in the Magnetic and Superconducting Materials group in Leiden university from March 2005 until August 2005 under supervision of Prof Dr. J. Aarts, Ing. R. W. A. Hendrikx and Ing. M. B. S. Hesselberth

Contents

Chapter 1

Introduction

Permalloy is an alloy with the special property that it requires a very weak magnetic field to let it switch the direction of magnetization compared to other ferromagnetic materials, combined with a high M_s (saturation magnetization) and low magnetostriction. For this reason it several possible applications are being researched, like the behaviour while in contact with a superconductor, or the possible usage as RAM memory in computers. Several groups have studied the magnetization of rectangle shaped structures[1, 2, 3, 4], others study circular dots[5, 6], switching behaviour of single domain elements[7, 8], or even more complex shapes[9, 10, 11]. In this project rectangle shaped microstructured permalloy elements have been studied. In particular, Bloch walls have been observed and the ends of 2 μm $\times$ 20 μm rectangles have been imaged. This has been done to give a better insight in the results of (future) experiments with superconductor/ferromagnetic (SF) hetero structures.

Chapter 2

Theory

All theory described in this chapter originates from reference [12], unless otherwise specified. For a more detailed explanation, the reader should refer to [12], or another book about magnetism.

When an external magnetic field is applied to a material, the magnetization inside the material may change. Some materials become magnetized parallel to the field, which is called paramagnetism, other materials show antiparallel magnetization, called diamagnetism. Both of these two effect are in general relatively weak and disappear once the external field is turned off.

The work described here is done on another type of magnetism, called ferromagnetism. Ferromagnetic materials do not only align their internal magnetic moments in the direction of the applied field, they also remain magnetized after the field is removed and show spontaneous magnetization. On a microscopic scale a ferromagnet consists of domains. Within a domain the magnetization is in one direction, but neighbouring domains are magnetized in other directions, resulting in a net zero magnetization on the macroscopic scale. When a field is applied, the domains in the same direction as the field either become larger at the expense of their neighbours, or domains in other directions rotate towards the direction of the field. Once the field is turned off, these domains may remain in the same directions. The macroscopic behaviour of a magnet is often described in a hysteresis loop. A typical hysteresis loop is shown in figure 2.1.

2.1 Ferromagnetism

Before the existence of domains can be explained, it is first necessary to explain the fundamental physics behind ferromagnetism and the energies that play a role in determining the behaviour of a ferromagnet. In particular,

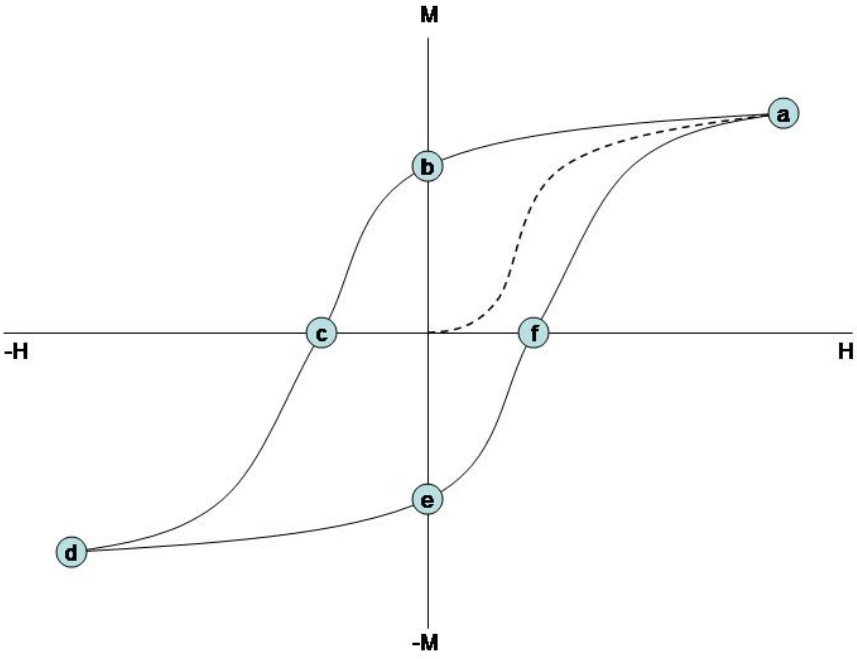

Figure 2.1: *Typical hysteresis loop for a ferromagnetic material. The material is demagnetized at zero field. Once a magnetic field (H)is applied the magnetization will follow the 'virgin' curve until saturation (M_S) has been reached (point a). When the field is turned down, the remaining magnetization at zero field is called remanence (point b). The opposite field required to demagnetize the sample is called the coercive field (point c). If the field is increased further in the opposite direction, the sample will saturate in that direction (point d).*

exchange energy will get a thorough explanation, since this is the energy that 'creates' ferromagnetism.

2.1.1 Origin of exchange energy

Two electrons

When two electrons are in the same potential, the Pauli exclusion principle prevents those two electrons from being in the same state. This means that either their wave functions or their spin functions have to be antisymmetric. For weak electron interactions, the effect can be calculated using perturbation

theory.

$$\begin{aligned} E_S &= E^0 + C_{ij} + \mathcal{J}_{ij} \\ E_T &= E^0 + C_{ij} - \mathcal{J}_{ij} \end{aligned} \tag{2.1}$$

Here E_S and E_T are the singlet and triplet state energies, E^0 is the unperturbed energy, C_{ij} is the Coulomb energy and $\mathcal{J}_{ij}$ is the exchange energy of the two electrons in states i and j. $\mathcal{J}_{ij}$ is given by:

$$\mathcal{J}_{ij} = \int \phi_i^*(1)\phi_j^*(2)\frac{e^2}{4\pi\varepsilon_0 r_{12}}\phi_i(2)\phi_j(1)dv \tag{2.2}$$

ϕ_i and ϕ_j are the wave functions for corresponding to the states i and j. If the Coulomb interaction is strong, C_{ij} and $\mathcal{J}_{ij}$ can no longer be considered perturbations on the energy E_0, the ground state becomes one of either parallel or antiparallel spin, depending on the sign of $\mathcal{J}_{ij}$.

Exchange in transition metals

In order to understand the physics of magnetism in the transition (3d) metals three concepts are needed.

The first is the broadening of atomic levels into bands in solids when the atoms get closer together, see figure 2.2a. The $4s$ electrons have a lower energy than the $3d$ electrons and are further away from the nucleus, they bond more when the interatomic distance increases. The lower half of a band contains mainly bonding states, the upper half contains mainly antibonding states. Figure 2.2b shows a broad s band and a narrow d band.

The second concept is the internal field $H_E = \lambda M$ caused by the Coulomb interaction (to be exact, the exchange integral $\mathcal{J}_{ij}$) that occurs as a result of the Pauli exclusion principle. This interaction shifts the spin up and spin down parts of the d band relative to each other, as in figure 2.2b. A simple way of understanding magnetic exchange in metals is by comparing it to Hund's first rule in atoms; in degenerate states the parallel spins are filled first to have a minimal spatial overlap. In a band however, states are not degenerate; it costs energy to put all electrons in the spin up band. The energy cost is greater if the density of states $Z(E)$ is small, that is, they are spread out over a broad energy range. This leads to the Stoner criterion for the occurrence of magnetism, formula 2.3.

$$\mathcal{J}(E_F)Z(E_F) > 1 \tag{2.3}$$

The last concept is that bonding states favour paired, antiparallel spins, antibonding favours parallel spins. The first half of a band is bonding, that's

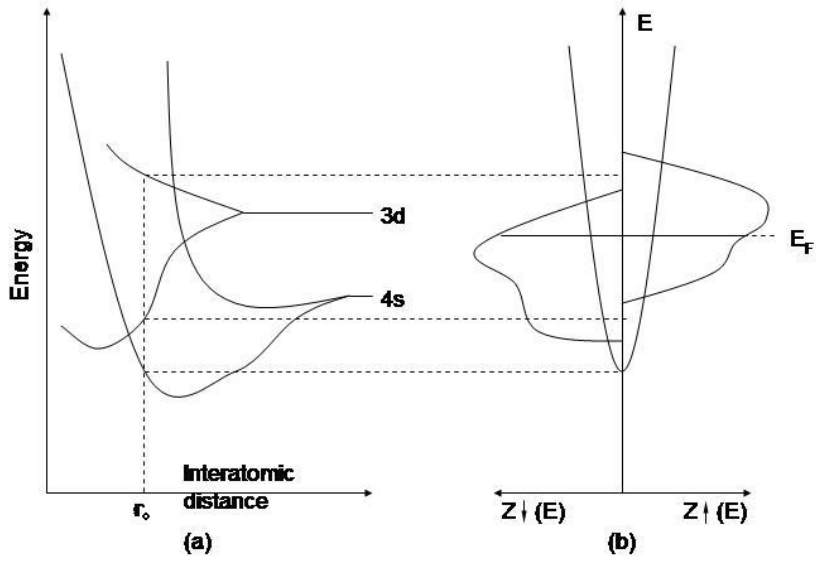

Figure 2.2: *(a)Evolution of atomic 4s and 3d states at large interatomic spacing to bands at smaller spacing (r_0 occurs when the net repulsive force $-\partial E/\partial r$ from 4s electrons exactly balances the net attractive force from 3d electrons); (b) density of states of 4s and 3d states split to reflect exchange preference for spins of one direction. Magnetism occurs if the Fermi energy E_F[13] lies within the d band. Taken from [12]*

why ferromagnetism does not occur in the first half of the $3d$ transition metals (V, Cr, Mn), but does occur in the second half of the $3d$ series (Fe, Co, Ni).

2.1.2 Energies in ferromagnetism

Exchange energy

The discrete microscopic and the macroscopic energy density is given by formula 2.4, where A is the exchange constant, it represents the energy cost to change the direction of the magnetization, a is the lattice constant, M_S is the saturation magnetization, θ is the angle between two neighbouring spins and S is the spin. It is a short range effect, it is limited to direct neighbours.

$$f_{ex} = -\frac{2\mathcal{J}S^2}{a^3}\cos\theta_{ij} = A\left(\frac{\partial\theta}{\partial x}\right)^2 \rightarrow A\sum_{i=1}^{3}\left(\frac{\nabla M_i}{M_S}\right)^2 \tag{2.4}$$

Magnetostatic energy

Magnetostatic energy originates from discontinuities in the normal component of magnetization across an interface. It is given in formula 2.5. This effect is long range, it is generally much smaller than exchange energy at an atomic scale, but can become much larger in larger volumes at a longer range. At the edges of a magnet, or for small structures it is the energy that causes shape anisotropy.

$$f_{ms} = -\mu_0 M_S \cdot H_i = \frac{\mu_0}{2} M_S^2 \cos^2\theta \tag{2.5}$$

Magnetocrystalline anisotropy

Magnetocrystalline anisotropy means it costs less energy to magnetize the sample in a particular direction compared to other directions. It originates from the crystal structure; in certain directions the distance between atoms is different compared to other directions. This favours magnetism in the so called easy directions. It is given in equation 2.6, K is the anisotropy constant, α is a direction cosines.

$$\begin{aligned} f_a &= K_2 \sin^2\theta + K_4 \sin^4\theta + \ldots (uniaxial) \\ f_a &= K_1(\alpha_1^2\alpha_2^2 + \alpha_2^2\alpha_3^2 + \alpha_3^2\alpha_1^2) + K_2\alpha_1^2\alpha_2^2\alpha_3^2 + \ldots (cubic) \end{aligned} \tag{2.6}$$

Magnetoelastic energy

Magnetoelastic is a type of magnetocrystalline anisotropy that is proportional strain. For cubic materials it given in equation 2.7, for isotropic materials it is given in equation 2.8, B_i is the magnetoelastic constant, e is the strain constant.

$$\begin{aligned} f_{me}^c =& B_1[e_{11}(\alpha_1^2 - \frac{1}{3}) + e_{22}(\alpha_2^2 - \frac{1}{3}) + e_{33}(\alpha_3^2 - \frac{1}{3})] \\ &+ B_2(e_{12}\alpha_1\alpha_2 + e_{23}\alpha_2\alpha_3 + e_{31}\alpha_3\alpha_1) + \ldots \end{aligned} \tag{2.7}$$

$$f_{me}^{iso} \approx B_1 e_{33} \sin^2\theta = \lambda_S^2 E \cos^2\theta = \frac{3}{2}\lambda_S \sigma \cos^2\theta \tag{2.8}$$

Induced anisotropy

When a magnetic field is present during the sputtering process (see Appendix), it may induce anisotropy. This will favour magnetization in the direction of the field.

Zeeman energy

Finally, there is the Zeeman energy, the energy of a magnetic moment in a field, given for both a single moment and per unit volume in equation 2.9.

$$\begin{aligned} F &= -\mu_m \cdot B \,(single\ electron) \\ f_{Zeeman} &= -\mu_0 M \cdot H \,(energy\ per\ unit\ volume) \end{aligned} \tag{2.9}$$

2.1.3 Permalloy

Permalloy, with a composition of 78% nickel and 22% iron has the property that both the magnetocrystalline and the magnetostriction anisotropy pass through zero near this composition. Since both of these effects are very weak it is possible to change the magnetization direction in permalloy with a much smaller field than other ferromagnets. Permalloy has an uniaxial magnetocrystalline anisotropy (K_2 in formula 2.6 is often callled K_u), however, due to the sputtering process on a silicon substrate, the easy direction varies throughout the sample. Induced anisotropy, on the other hand, may play an important role.

2.2 Domains and domain walls

Now that we have the relevant energies, we are now able to explain why domains are formed. While the exchange energy tries to align all moments in the same direction (figure 2.3a), in particular the nearest neighbours. The magnetostatic energy, which is long range, tries to prevent moments sticking out of an interface; this is the main energy that forces the creation of domains (figure 2.3b). To reduce the magnetostatic energy even further, closure domains are formed (figure 2.3c). At this point anisotropy (from any source) begins to play a role. If there is a strong uniaxial anisotropy, it may be able to prevent the formation of closure domains, as this would force the magnetization into a hard direction. The opposite can also happen, if the easy magnetization direction is directed in the width of the rectangle, multiple closure domains may form, as in figure 2.3d.

Domain walls are often 180°, but in cubic materials, or low anisotropy uniaxial (like permalloy), domains can have 90° domain walls, although 71° or 109° are also possible in cubic materials if the easy axes are not in the $< 100 >$ directions. In a wall itself it's always more favourable to put some spins into the hard (high anisotropy energy) direction, resulting in a gradual change of direction, than an instant change the magnetization by of 180°,

which costs more exchange energy, since this is the highest energy at the atomic scale.

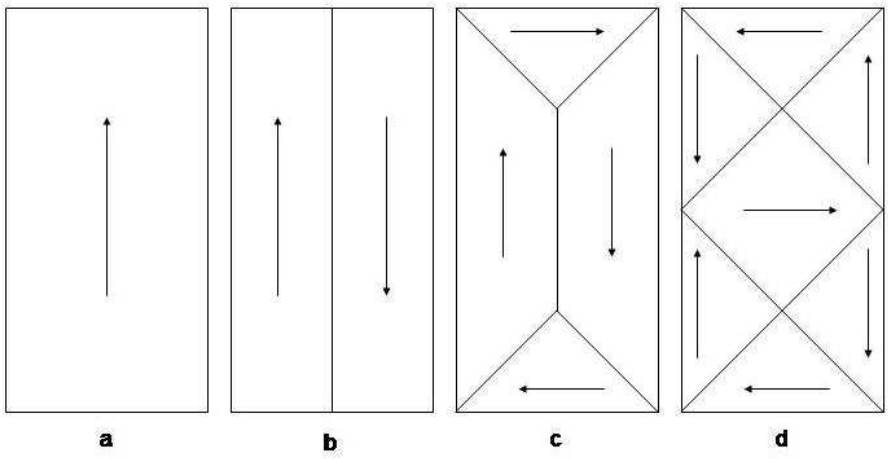

Figure 2.3: *A single domain structure can reduce it's energy by forming domains. (a) Single domain structure, (b) Two domain structure to decrease magnetostatic energy, at the expense of a domain wall, (c) the formation of closure domains to reduce the magnetostatic energy even further, (d) formation of smaller domains, which may reduce the total energy even further in some materials.*

Four types of 180° walls can be distinguished; Bloch, Néel, cross-tie and C-shaped walls, they are schematically displayed in figure 2.4.

2.2.1 Bloch walls

In a Bloch wall the magnetization rotates out of plane, creating 'free' poles at the top and the bottom of the sample. The surface energy density is given by:

$$\sigma = \int_{-\infty}^{\infty} \left[f_a(\theta) + A \left(\frac{\partial \theta}{\partial z} \right)^2 \right] dz \tag{2.10}$$

where f_a is the total anisotropy energy density, θ is the angle between the magnetization at z and the magnetization at $-\infty$ and z is perpendicular to the wall in the plane, which reduces to $\sigma_{dw} = 4(AK_u)^{1/2}$ for uniaxial materials (like permalloy). For uniaxial materials the magnetization direction, as function of z is given by:

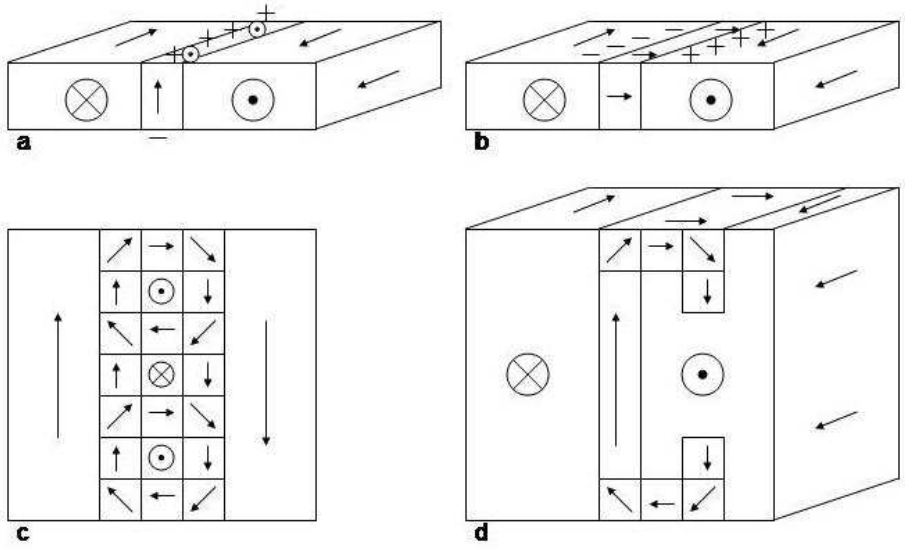

Figure 2.4: *Four different types of walls. (a) A Bloch wall, in this type of wall the magnetization rotates out of plane. Magnetic 'charge' (causing magnetostatic energy) is building up at the top and bottom of the wall, indicated by + and - signs, (b) A Néel wall, the magnetization rotates in the plane of the sample, creating magnetic 'charge' at the sides of the wall, (c) A cross-tie wall (top view). In order to reduce the magnetostatic energy, the wall direction alternates, having both Bloch and Néel like parts, (d) An asymmetric Bloch wall, also known as a C-shape wall. At the center it is like a Bloch wall, but at the top and bottom it behaves like a Néel wall. The magnetization rotates even a bit further, creating another vertical component, which reduces the magnetostatic energy in the z-direction.*

$$\theta(z) = \operatorname{arccot}\left[\sinh\left(\frac{\pi z}{\delta_b}\right)\right] + \pi = \arctan\left[\sinh\left(\frac{\pi z}{\delta_b}\right)\right] + \frac{\pi}{2} \tag{2.11}$$

δ_b is the domain wall thickness and is given by:

$$\delta_b = \pi\left(\frac{A}{K_u}\right)^{1/2} \tag{2.12}$$

2.2.2 90° walls

90° walls (or in some materials 71° or 109°) are very common near the corners of microstructured materials with a cubic anisotropy and low uniaxial

anisotropy, where closure domains are formed. They are visible in figure 2.3 c and d. 90° walls are always in the plane of the film.

2.2.3 Néel walls

In thin films, the magnetostatic energy density increases rapidly [14] since the charged area at the top and bottom of the sample increase compared to the wall area. In order to reduce the total energy, it is more favourable to rotate within the plane. At thicknesses close to the boundary thickness this will increase the magnetostatic energy, but will significantly lower the exchange energy. In even thinner films both forms of energy are lower than in a Bloch wall. For $t \ll \delta_M$ The energy density can be approximated as:

$$\sigma_N \approx \pi t M_S^2 \tag{2.13}$$

and the wall thickness can be approximated as:

$$\delta_N \approx \pi \left(\frac{2A}{K}\right)^{1/2} \tag{2.14}$$

2.2.4 Cross-tie walls

In order to reduce the magnetostatic energy in both Néel and Bloch walls, the magnetization direction alternates in a cross-tie wall, as illustrated in figure 2.4c. This type of walls are typically found in the intermediate thickness between a Néel wall and an asymmetric Bloch wall. If it is assumed that the magnetization does not change throughout the thickness of the film, but only within the plane of the film itself, this wall has less energy than a Bloch wall[15].

2.2.5 Asymmetric Bloch walls (C-shaped walls)

A C-shaped wall is like a Bloch wall in the bulk, but like a Néel wall at the surfaces. By creating Néel like walls at the top and the bottom and rotating the magnetization even a bit further in the opposite direction of the Bloch part of the wall, the magnetostatic energy is minimized. This wall is found in thicker films[14] in simulations and using MFM by Barthelmess et al[2]. No analytical calculation of its energy has been found in the literature so far, but simulations do exist[14].

Chapter 3

Magnetic Force Microscopy

The measurements on the samples has been done using magnetic force microscopy (MFM). This is a special type of atomic force microscopy (AFM) which does not measure the topography but the magnetic field perpendicular to the sample. First topography scans have been made using tapping mode AFM, followed by an MFM measurement where the tip was kept above the surface, instead of touching the surface. The AFM used in these experiments was a commercial Nanoscope from Digital Instruments, but instead of using the default hardware and software, an 'SPM 100' controller from RHK Technology Co. with 'SPM 32' software has been used.

3.1 Atomic Force Microscopy

An AFM scans the surface using a small cantilever with a sharp tip. A laser beam reflects from the back of the cantilever towards 2, 4 or more photodiodes, depending on the model, which allows the detection of the cantilever deflection, as illustrated in figure 3.1. The scanning is done line by line using piezoelectric actuators (piezos), which allows sub-Å movement in both the lateral and vertical directions. There are several methods of measuring a sample with an AFM, the most common are contact and tapping mode. A feedback loop (usually PI, but sometimes PID controlled) keeps the deflection (in contact mode), or the oscillation amplitude (in tapping mode) constant by adjusting the tip-sample distance with the z-piezo.

3.1.1 Contact mode

In contact mode the tip is brought into direct contact with the sample, keeping the cantilever slightly bent. Depending on the surface topography the

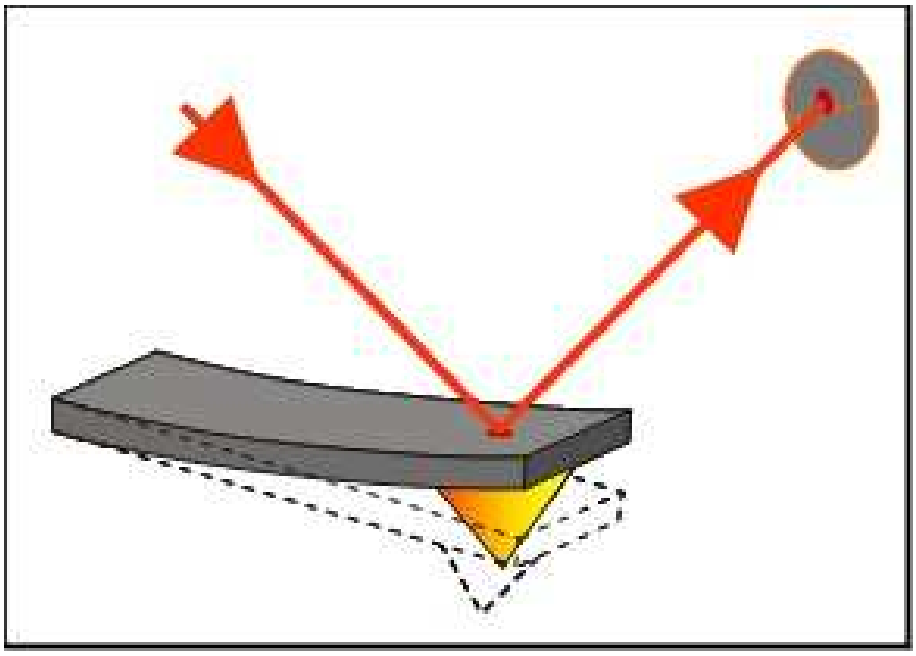

Figure 3.1: *Typical detection method of the cantilever deflection in an AFM, a reflected laser beam gets detected by photo diodes. Taken from [16]*

cantilever bends up- or downwards, which will move the laser spot on the photodiodes. The feedback will then move the sample up or down with the z-piezo to keep a constant deflection.

3.1.2 Tapping mode

In tapping mode the cantilever is driven close to mechanical resonance, generally slightly below it's resonance frequency, at the frequency where $\partial A/\partial f$ is the largest. When the tip gets close to the sample it will hit the sample, which has a dampening effect on the oscillation. The amplitude during 'contact' changes as a result of the topography. Just like in contact mode, the feedback will move the sample up or down to keep this amplitude at a constant level, typically 50% of the amplitude in free space.

3.2 Magnetic Force Microscopy

When measuring the magnetic field, the tip is brought into resonance, but unlike tapping mode, it does not hit the surface. The tip of the cantilever,

coated with a magnetic material (during most of the measurements this was Co), is often considered a point dipole for simplicity. The force on the dipole $\mathbf{m_1}$ on the cantilever as results of a dipole $\mathbf{m_2}$ in the sample is given by:

$$F = \nabla \left(\frac{3(\mathbf{m}_1 \cdot \hat{\mathbf{r}})(\mathbf{m}_2 \cdot \hat{\mathbf{r}}) - \mathbf{m}_1 \cdot \mathbf{m}_2}{r^3} \right) \tag{3.1}$$

However, in resonance, it is not the force, but the force gradient which is being detected. A force gradient changes the effective spring constant:

$$c_{eff} = c - F' \tag{3.2}$$

which in turn changes the resonance frequency:

$$\omega_0' = (c_{eff}/m)^{1/2} \approx \omega_0 \left(1 - \frac{F'}{2c} \right) \tag{3.3}$$

The approximation is valid if F' is small compared to c. Figure 3.2 gives a illustration what happens to the oscillation as a results of a force with a non zero spatial derivative. The shift of resonance frequency changes the amplitude and phase of the oscillation, which can be detected by a lock-in amplifier. Measuring the phase gives slightly better (a factor of $\sqrt{2}$) better signal to noise than the amplitude.

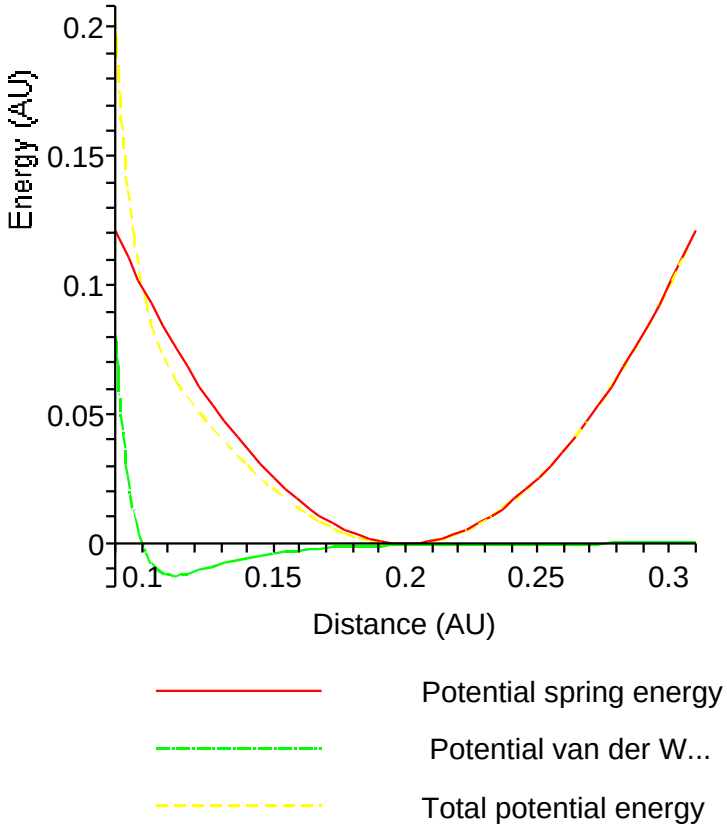

Figure 3.2: *A spring in a van der Waals potential. In the attractive regime the parabola becomes wider as a results of the van der Waals potential, thus changing the effective spring constant. This does not apply to just van der Waals forces, but to any force that has a non zero derivative.*

Chapter 4

Results

There are many unknown factors during MFM measurements. The most important uncertainty is the exact location of the magnetic moment on the tip, and how much each part of the tip contributes to the total signal, the average tip sample distance, and the exact oscillation amplitude. For this reason, the strength of the field is not calculated from the images. The images in this section only give information about the domain structure within the sample, not about the strength of the field (or rather, it's second derivative). To calculate the actual field it is more convenient to use a computer simulation to calculate the magnetization on a similarly magnetized sample and calculate the magnetic field using that data, similar to what has been done by Barthelmess et al [2].

For all figures in this section the top left (a) is the topography, the top right (b) is the corresponding MFM measurement and the bottom image (c) is a schematical representation of the domains within the sample, unless otherwise specified. Due to non- linear effects in the x- and y-piezos the distances given in the figures in this chapter are not correct. All lateral distances given are how they appear in the image. In reality they could be as much as 20% smaller.

4.1 50 nm permalloy

Figure 4.1 and 4.2 are results of a measurement of 50 nm thick permalloy. These are some early results, the quality of the images is not as good yet as those that will appear later in this chapter.

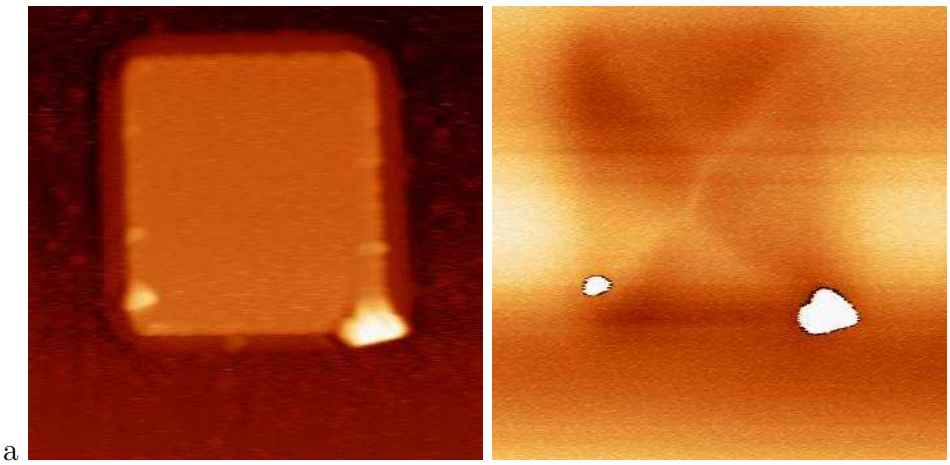

a b

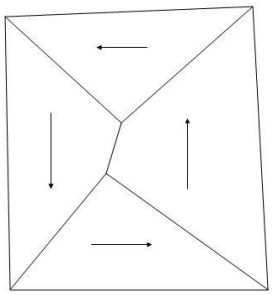

c

Figure 4.1: Topographic and MFM image of a $2\mu m \times 2.5\mu m$ element. A short Bloch wall can be seen, which can be recognized because it's straight, with a clear contrast.

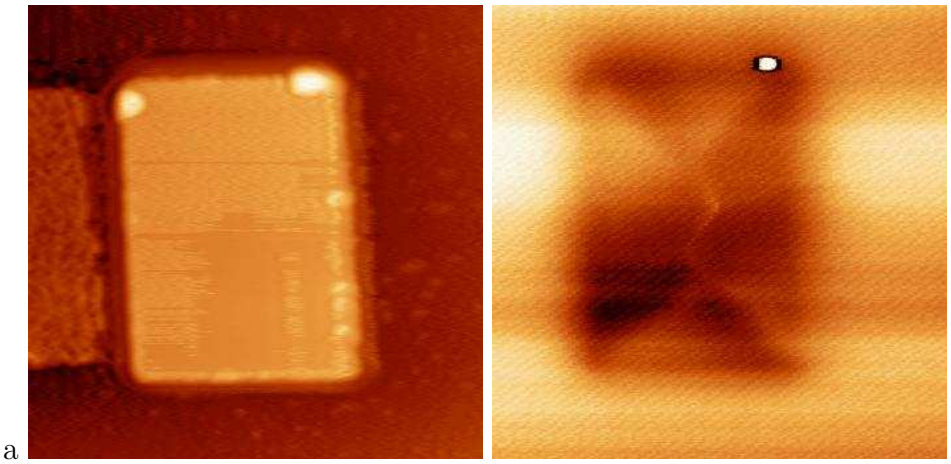

a b

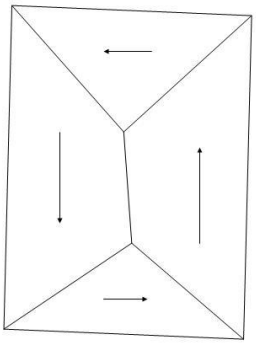

c

Figure 4.2: Topographic and MFM image of a $2\mu m \times 2.8\mu m$ element. A cross-tie wall is visible, because a cross-tie wall extends into the domains, therefore, it is not a straight line.

4.2 100 nm permalloy

Figure 4.3, 4.4 and 4.5 are elements on a 100 nm thick permalloy sample. All observed 180° domain walls are in the y-direction (some images are slightly rotated). This could be the result of induced anisotropy caused by the magnetic field inside the UHV, but it can also be coincidence. It is unknown in which direction the sample was orientated during the sputtering process.

a 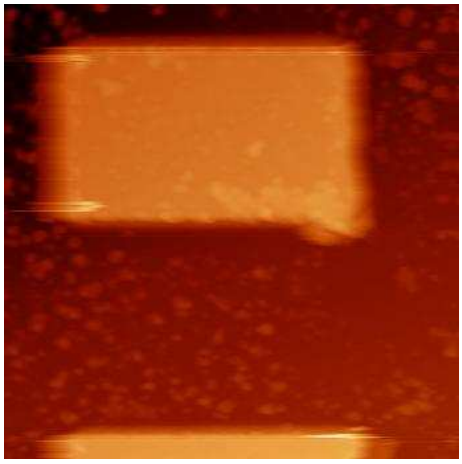 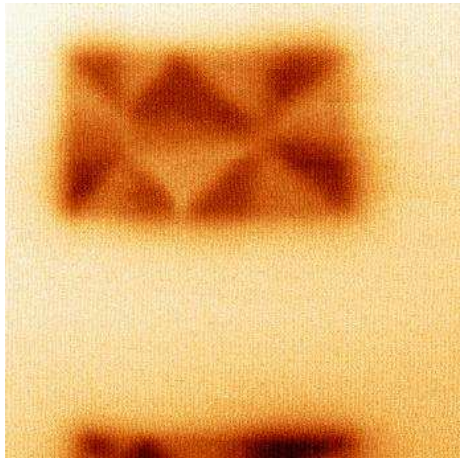 b

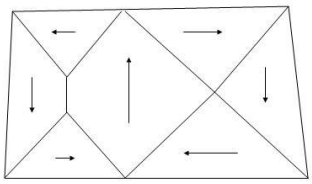

c

Figure 4.3: This $2.8\mu m \times 2\mu m$ elements has 7 domains. At the left side a short Bloch wall can be seen and at the right side a cross where four 90° walls come together.

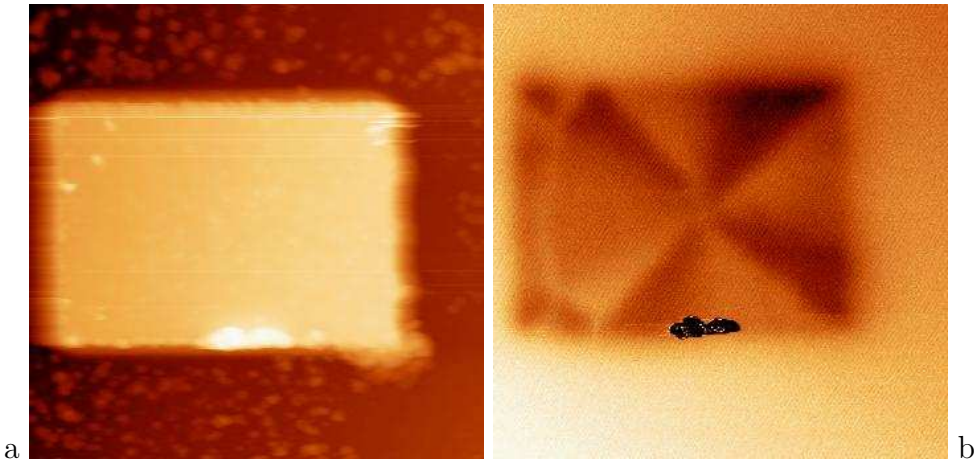

a b

c

Figure 4.4: $2.8\mu m \times 2\mu m$ element. A long Bloch wall at the left and a cross at the right side.

a 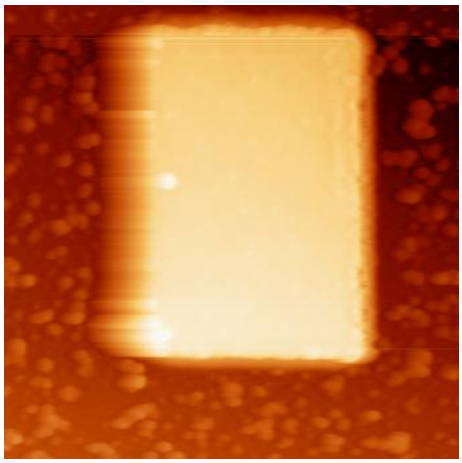 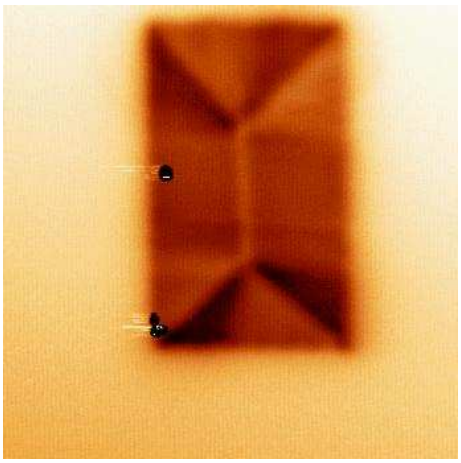 b

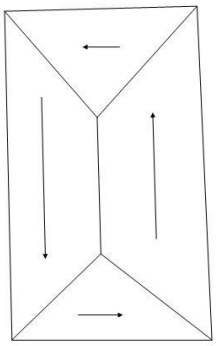

c

Figure 4.5: Bloch wall in a $2\mu m \times 3\mu m$ element.

4.3 100 nm permalloy with 20 nm Niobium

To prepare for future experiments concerning the interaction of domain walls with superconductors a sample with a $20nm$ thick layer of niobium on top of $100nm$ permalloy has been made. This sample contains both $2\mu m \times 20\mu m$ elements and elements with both sides approximately $2\mu m$.

In these images the oscillation amplitude of the cantilever has been reduced to $\approx 10nm$ (see appendix). On several MFM pictures some dark lines with a width of $\approx 20nm$ have been observed, often even away from the elements. It is unknown where they come from. Possibilities could be a tip effect, but such effect would be expected to be visible on the topographic image as well, or the formation of iron whiskers, but then the lines should be straight. Similar lines were also measured later on a sample with permalloy only (not shown).

4.3.1 Small structures

The same small structures were made on 100 nm permalloy with 20 nm niobium as on the previous permalloy sample. This was done to see whether the same magnetization patterns could be seen. Even though there was an applied magnetic field in the UHV, there was no evidence in the images that there was any induced anisotropy, since two elements which were rotated 90◦ in respect to each other showed the same magnetization pattern. Some results are displayed in figures 4.6, 4.7 and 4.8.

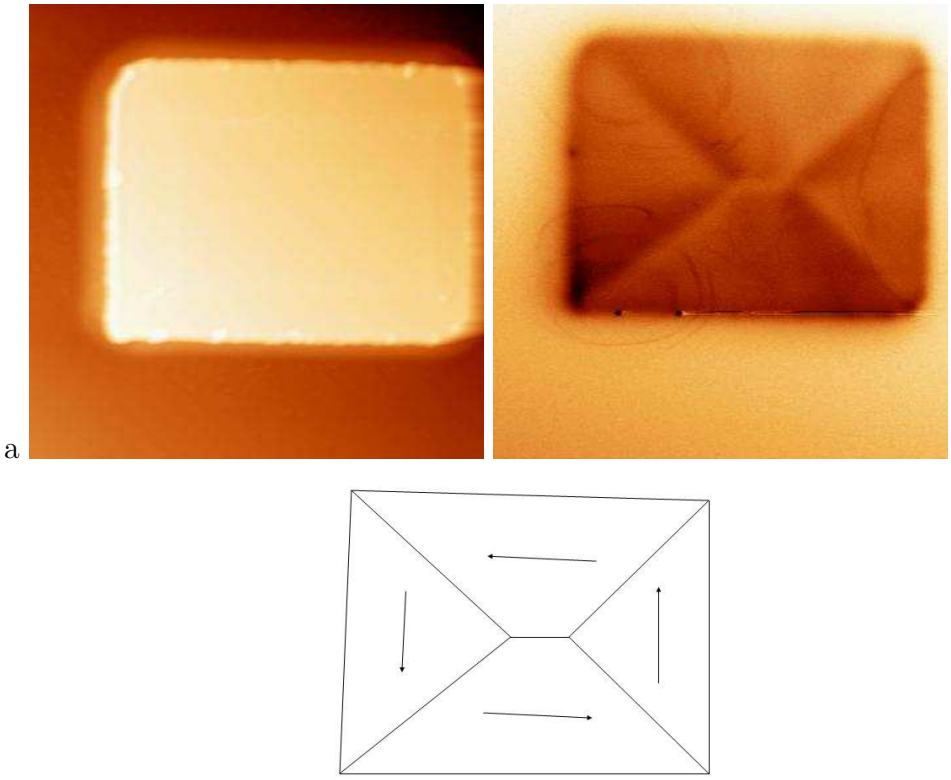

Figure 4.6: Bloch wall in a $3.5\mu m \times 2.5\mu m$ element, dark lines of unknown origin are visible at both left corners and the right side.

a 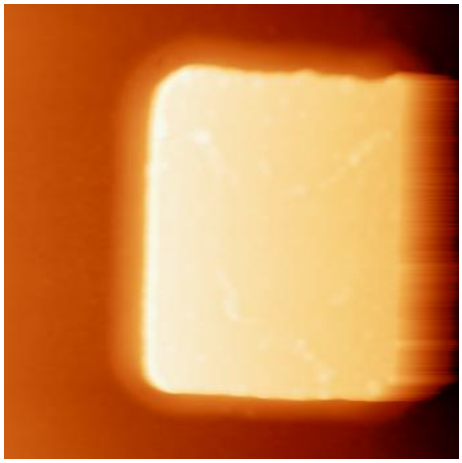 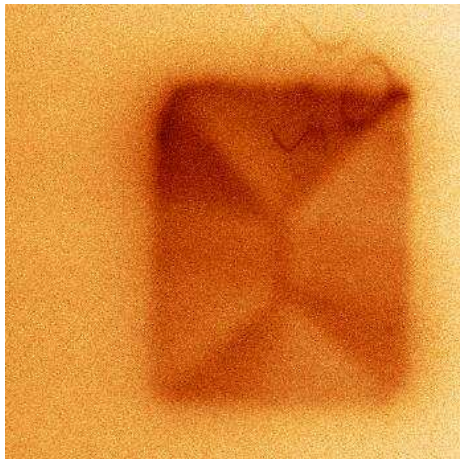 b

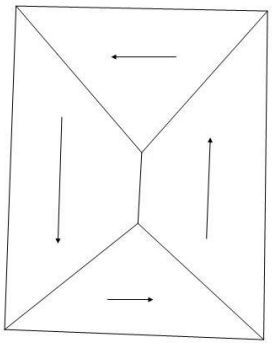

c

Figure 4.7: Bloch wall in a $2.3\mu m \times 2.6\mu m$, some dark lines are visible at the top of the element.

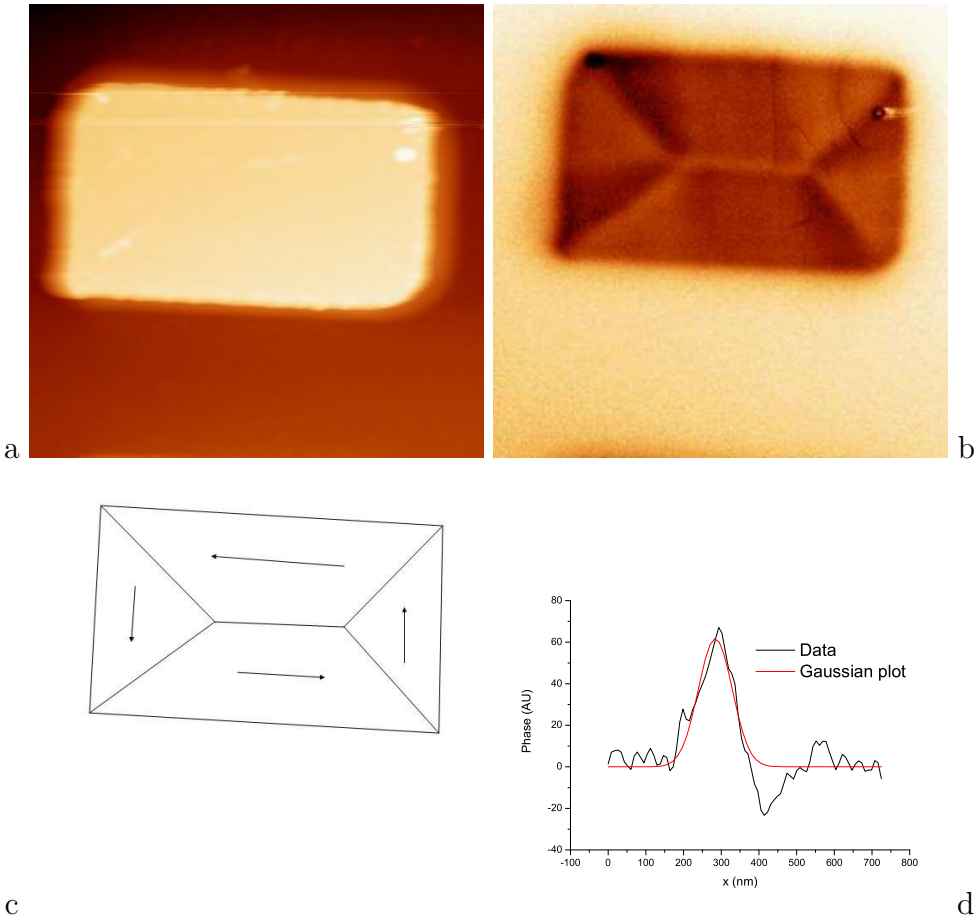

Figure 4.8: Another Bloch wall on a 3.5 $\mu m \times 2.0\ \mu m$. Due to the absence of drift during this scan, it was possible to scan at a distance of approximately 10-20 nm from the sample, a total distance of 30-40 nm from the permalloy. The wall profile taken shows a FWHM of 62 nm at this distance for the main peak, but also shows a small negative peak, indicating that the wall is not a perfect Bloch wall (figure 2.4b), but an asymmetric (C-shaped) Bloch wall (figure 2.4d).

4.3.2 2 μm $\times$ 20 μm structures

Since many SF experiments in this lab are done on 2 μm $\times$ 20 μm magnetic structures, some MFM images have been made on elements with that shape. They are displayed in figures 4.9, 4.10, 4.11 and 4.12. Most images have several domains at the ends, where they may be under the influence of the stray fields of neighbouring elements, but only one large in the center, which is caused by shape anisotropy. For these images, the full scan range of the AFM (8.3μm) has been used.

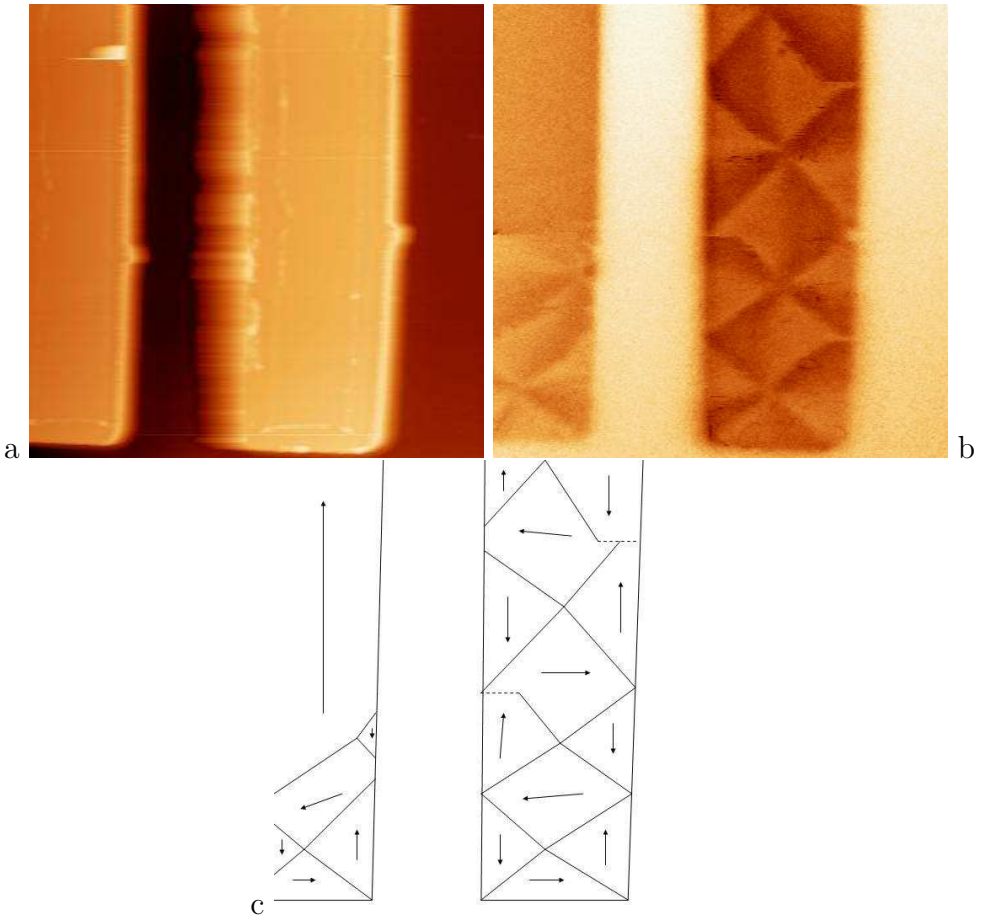

Figure 4.9: Two ends of 2 by 20 μm elements. The left element has only domains at the end, while the right has domains at the entire scanned region. Both elements show some evidence that the magnetization has been changed during the scan, indicated by the dotted lines. There is a difference in contrast between the elements, this has been caused by a plane fit, automatically done by the software (WSxM) which has been used to process the images, not by the scanning itself.

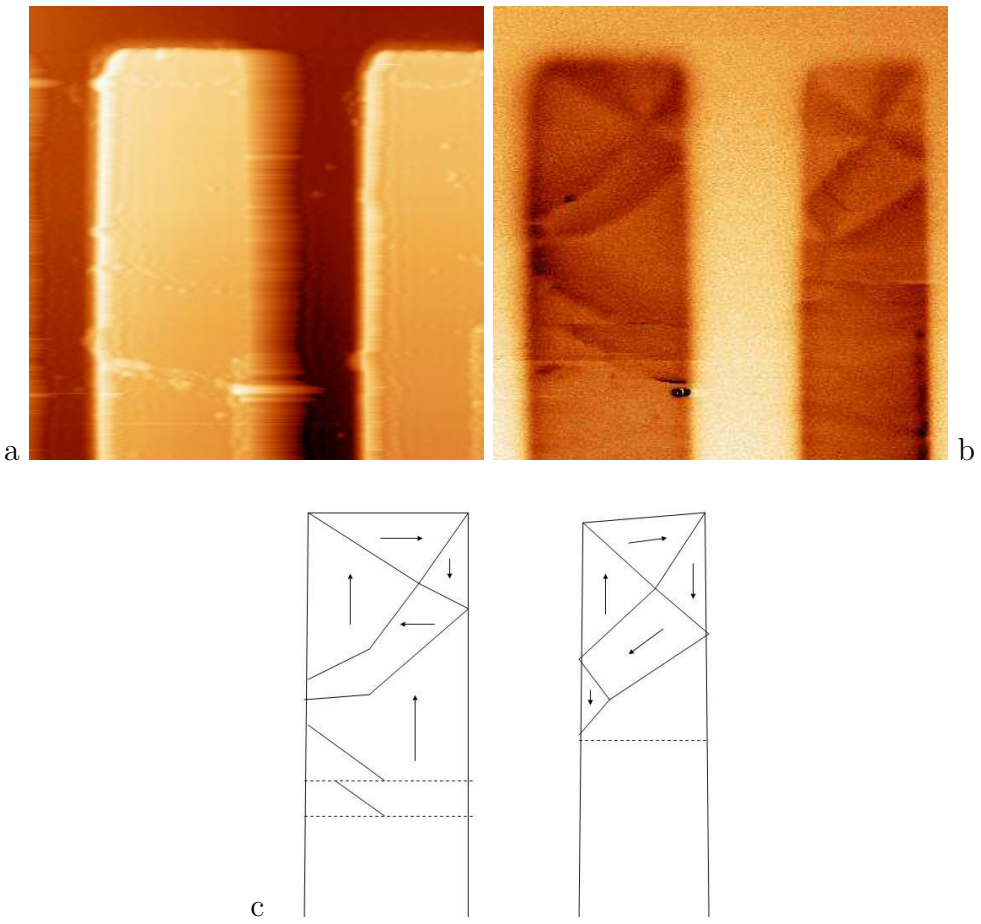

Figure 4.10: Two ends of 2 μm $\times$ 20 μm elements. The magnetiztion of the left element has been altered twice during the scan, indicated by the dotted lines.

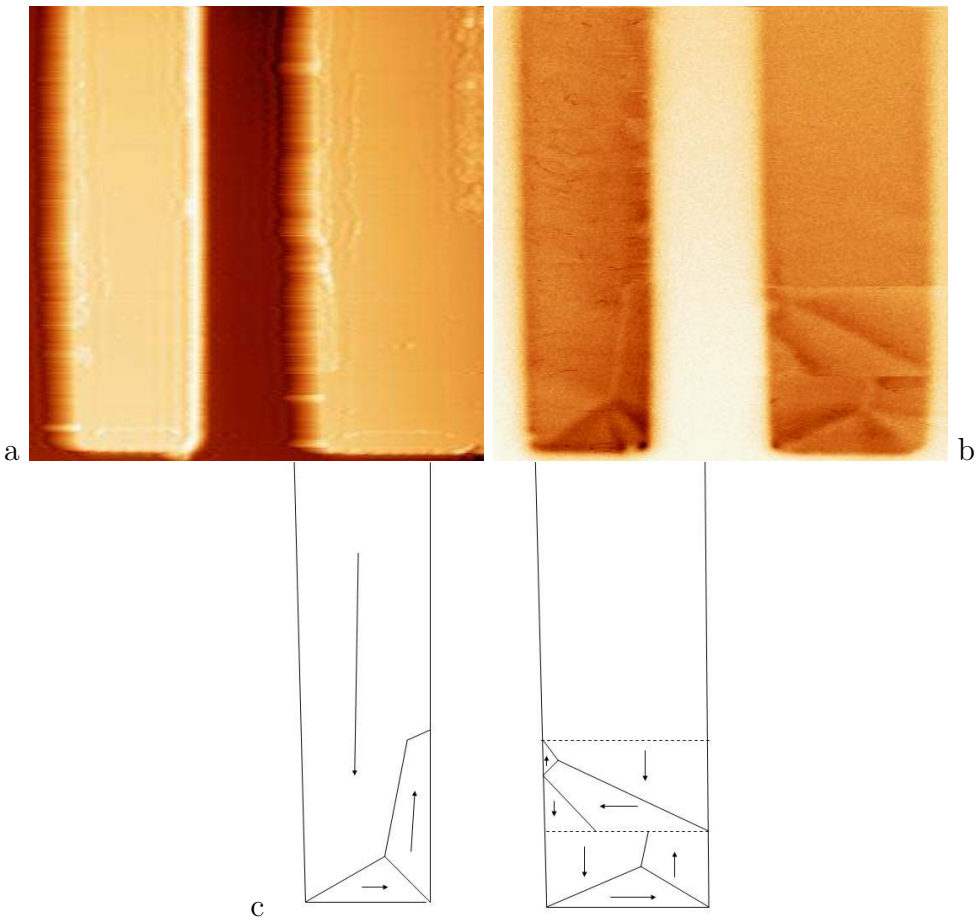

Figure 4.11: Two ends of 2 μm $\times$ 20 μm elements. None of these two show any domain structure towards the center.

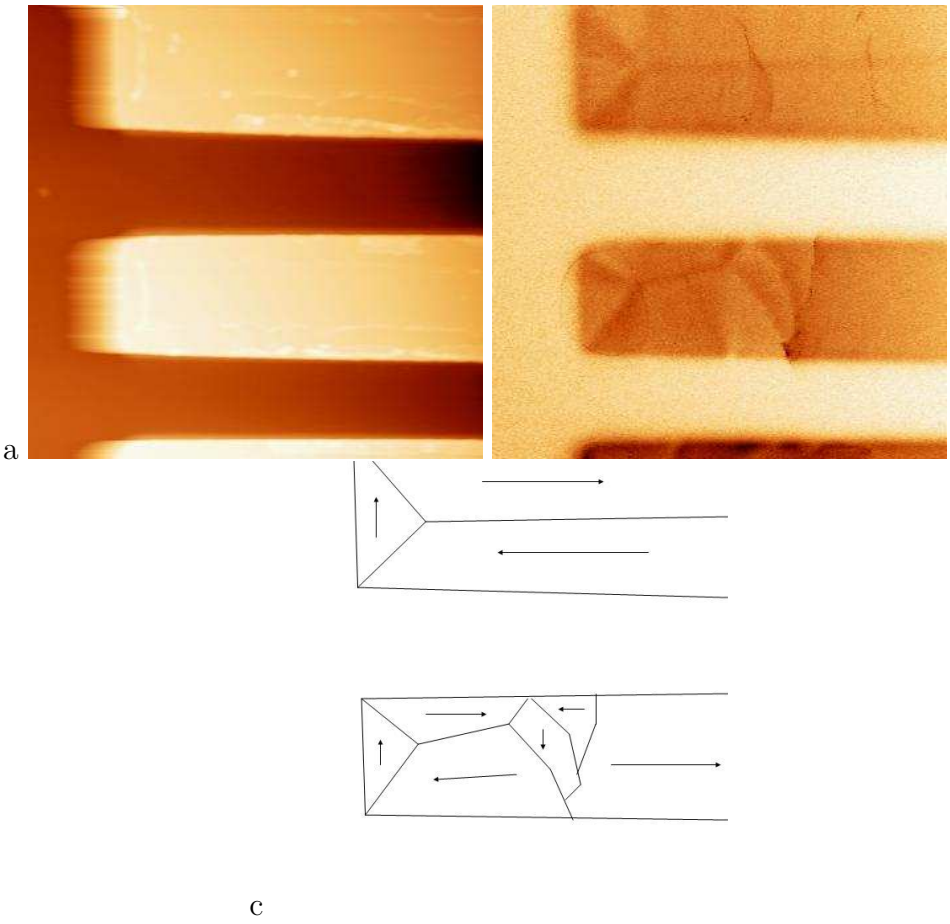

Figure 4.12: Two ends of 20 μm $\times$ 2 μm elements. The top element has a long Bloch wall. There are some dark lines, in the lower element it's not entirely clear whether a domain wall, or a dark line is visible.

Chapter 5

Conclusion

Bloch walls and the magnetic domain structure have been observed in 100 nm thick microstructured permalloy. Although the direction of these walls was not completely reproducible, it is certain they do appear in rectangles with dimensions of 1.5 $\mu m \times 2$ μm, 1.5 $\mu m \times 2.5$ μm and 2 $\mu m \times 2.5$ μm. The magnetic signal was also very clearly visible with a 20 nm thick niobium layer on top of the permalloy. the ends of 2 $\mu m \times 20$ μm have been imaged, the magnetization varies greatly from element to element, which may be related to strain or anisotropy, but also their close proximity to each other may have affected the magnetization.

Strange lines, with a width of approximately 20 nm have been observed on some elements after making the measurement method more sensitive. They were reproducible in repeating scans, but appeared to be randomly placed and in some cases not even above the element itself. No explanation for this effect has been found yet.

Appendix A

Sample preparation

The creation of the sample has 3 main steps which are explained in detail below. A schematic overview of the production process is given by figure A.1.

A.1 Sputtering

The samples have been sputtered in a home-built UHV magnetron sputter system, which has a base pressure that can be as low as $1.0 \times 10^{-10} mbar$, but is typically $1.0 \times 10^{-10} mbar$. During sputtering, highly energetic argon ions bombard a target, causing particles to break off, which then redeposit on the sample. The sputter conditions for permalloy are an argon pressure of $6.0 \times 10^{-3} mbar$ and a current of $200 mA$. The niobium has been sputtered with an argon pressure of $4.0 \times 10^{-3} mbar$ and a current of $220 mA$. To measure the thickness a crystal monitor was used. By measuring the changing resonance frequency of this crystal, the amount of sputtered material on it can be determined. For permalloy $0.272 \pm 0.03 nm$ on the crystal corresponds with $1 nm$ on the sample. This has been measured using X-ray diffraction; after sputtering $15.7 \pm 0.1 nm$ on the crystal the sample thickness was $57.8 \pm 0.1 nm$. For niobium the sputter rate was approximately $9.3 \pm 0.1 nm$ on the crystal for $19 \pm 1 nm$ on the sample.

A.2 E-beam lithography

After sputtering a resist layer was spin coated on the sample. With an Scanning Electron Microscope the elements have been written on the sample. During the development of the resist only the places that have been exposed with the electron beam remain. To make sure the last bits of resist were

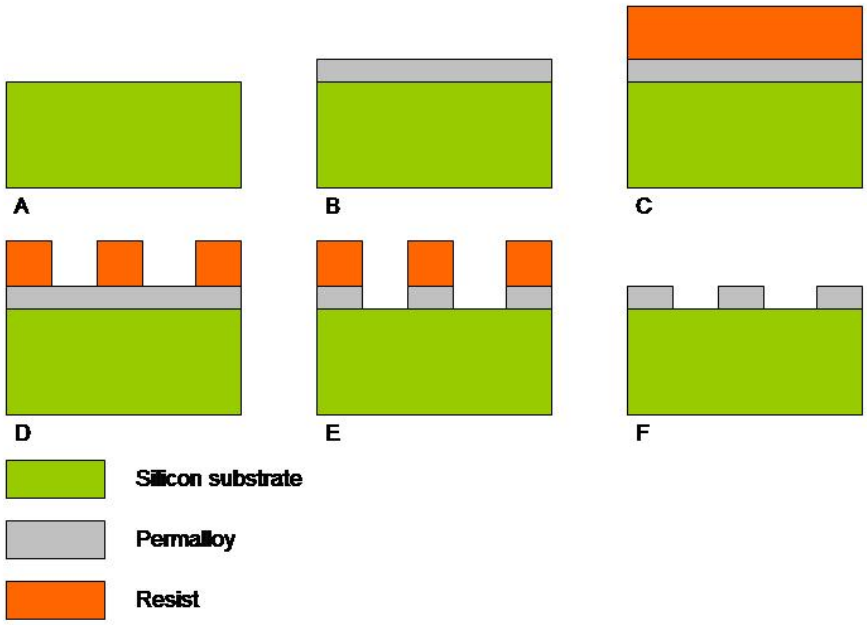

Figure A.1: *Preparation of the sample step by step. (a) A clean silicon wafer, 10-15 mm × 10-15 mm, (b) A sputtered layer of permalloy, possibly with a layer of niobium on top (not displayed), (c) a layer of resist gets spin-coated on top of the material, (d) after writing a structure with a SEM the developed resist is removed, (e) the permalloy (and niobium) is etched using an ion etcher, (f) the final result after solving the last resist in acetone.*

removed from the places where it should not be, the sample was put into an oxygen etcher. An oxygen plasma with a pressure of $1.0 * 10^{-1} mbar$ 'burned' the remaining unwanted resist away from the sample.

A.3 Ion-beam etching

After writing the pattern the sample was etched in an ion etcher. The base pressure is typically $1 \times 10^{-5} mbar$, argon is then added with a pressure of $2.5 \times 10^{-4} mbar$. In this etcher the sample is bombarded with argon ions, which will remove material except at the places where the resist is located, leaving the desired structure on the sample. The typical etch time is $30 sec$ for $10 nm$ of permalloy.

A.4 complications

A complication during this process is the formation of 'ears', displayed in figure A.2. These ears are formed when permalloy redeposits on the resist. A rotating sample holder, while etching under an angle should prevent this, but it did not. Several methods proved to be useful in removing those ears. The first (and best) method was reactive etching with bromine, similar to what others have done with chlorine[17]. First a gas of bromine with a pressure of $2.8 \times 10^{-4} mbar$ was inserted into the chamber, followed by argon for a total pressure of $5.0 \times 10^{-4} mbar$. The ears created by this process can easily be washed away with water, leaving nice flat edges. This method has been used on the $100nm$ permalloy sample.

The second method is using acid with Fe_3Cl to etch the ears away. The major disadvantage of this method is that it does not only etch the ears, but it also rounds all corners. Besides that, it can only be used if there is some protective layer on top of the structure, which could be the resist or any material that is unaffected by the acid. The acid used was concentrated HCl in water $(1 : 330 \pm 30)$ with $1.1 \pm 0.2 gram/240ml$ Fe_3Cl. This method has been used on the $100nm$ permalloy + $20nm$ niobium sample. The total etch time took a few minutes in an ultrasound. Both the exact concentration and time still needs to be optimized.

Another complication, which happened while making the sample with niobium, is that the resist remains between the ears. This has been removed in the oxygen etcher, which etched a total of 50 minutes, before acid had been used to remove the ears. It is not known how long it actually took to remove the resist.

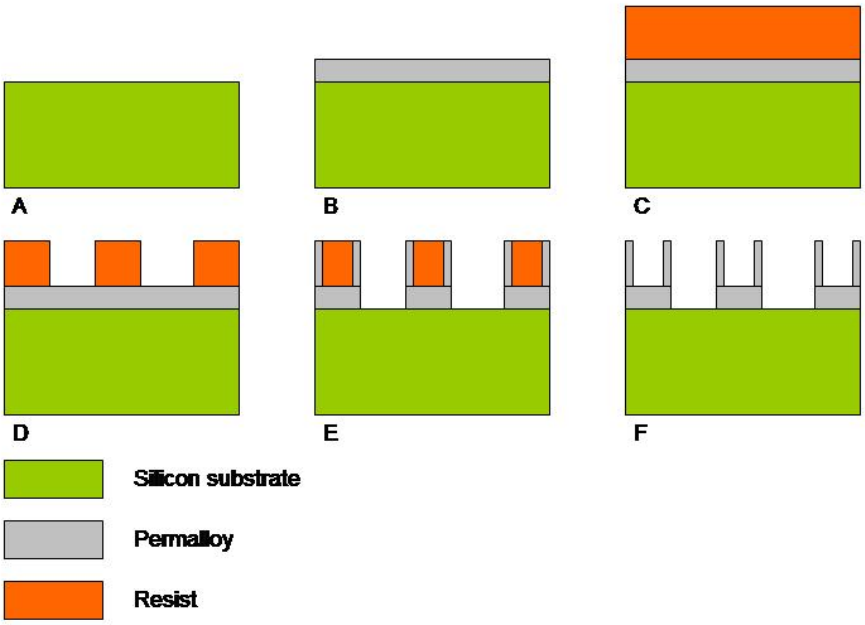

Figure A.2: *Preparation of the sample step by step. (a-d) Same as in figure A.1, (e) the permalloy redeposits on the resist during the etching process, (f) 'ears' on the sides of the structure after the resist has been removed.*

Appendix B

Quality of the MFM images

In addition to measuring the domain structure, one of the purposes of this project was to optimize the quality of the MFM measurements. Especially during the beginning of the measurements the quality of the images was rather poor, as shown in B.1.

The cause was too large a driving voltage, resulting in tip oscillations with an amplitude with an order of magnitude of 1 μm. The total signal (coming from the photodiodes was too large for the lock-in amplifier (max 1 V RMS) and was reduced by a factor 100, while the relevant signal (after subtracting an offset) had to be expanded 100 times again. This large amplitude was useful for topographic measurements, since the changes in topography are much less than the oscillation amplitude. However, for magnetic measurements a small oscillation gives a much larger (relative to the total amplitude) change in amplitude and phase because the average tip-sample distance can be significantly decreased. This can easily understood by recalling figure 3.2, if the parabola in the graph moves to the right (away from the surface), the tip spends more time at places where the field is much weaker and thus reducing the signal strength. During the last measurement the oscillation amplitude is reduced to approximately 10 nm by reducing the driving voltage. This resulted in a major improvement of the image quality, especially the phase signal, see for example figure B.2.

Furthermore, the lock-in settings have a lot of influence on the quality of the images, especially the 'time constant', this is the time over which the output signal is averaged before it is changed. A high time constant reduces noise (more time to average the signal) , but results in horizontal lines in the image (if the time to average over is more than the time for one pixel), which can be seen very clearly in figure B.1. Increasing the time constant and scanning slower could solve both of these issues, but becomes unviable due to drift in the z-direction. Drift can come from several sources, for example

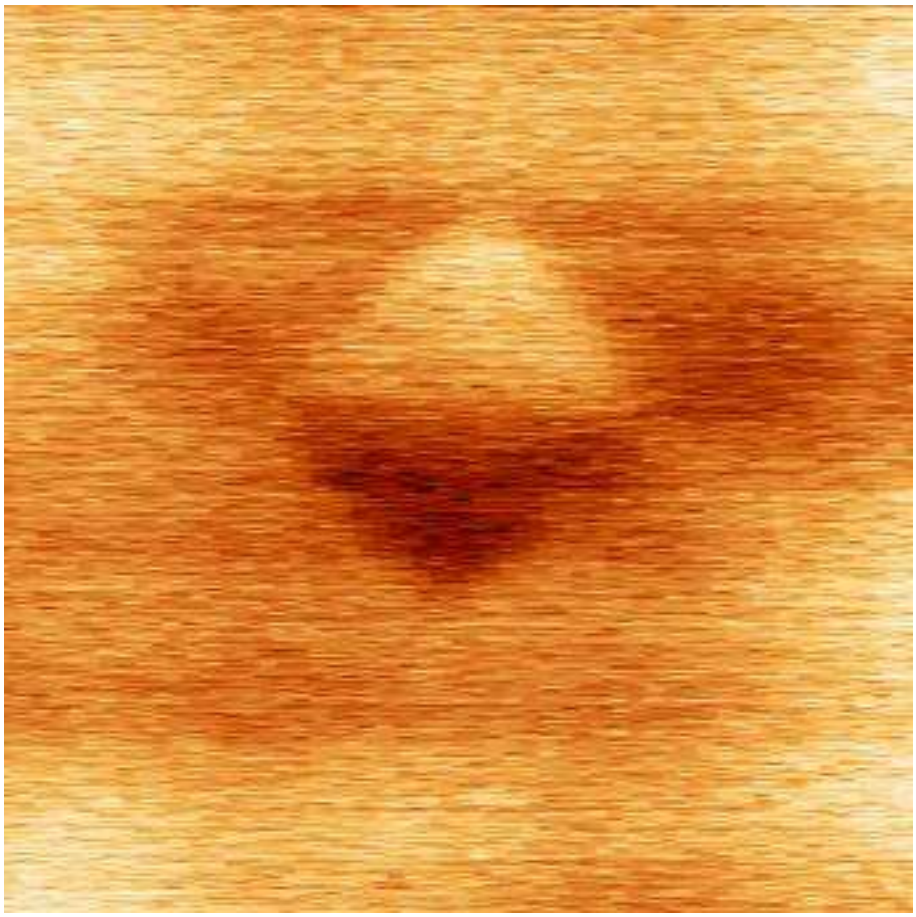

Figure B.1: *One of the first MFM measurements. This is the amplitude signal, which had to be expanded 100 times (after subtracting an offset signal) by the lock-in amplifier to get enough contrast. The phase signal did not have enough contrast to produce a clear image.*

the sample can become warm from the laser. Typical scan times for were 500 ms per line (1 ms per pixel) with a time constant of 30 μs. The total size of a picture is 512 $\times$ 512 pixels, which took 8.5 minutes.

There have also be a few measurements using 'Lift Mode' on another AFM. This was the same type of AFM, except this one had the original hardware and software. During Lift Mode each line is scanned four times, first the trace and retrace topology is scanned in a single line, then the tip is lifted to a set height and follows the exact same height curve along the same line. This is then repeated for each line in the image. The main advantage of this method is that it basically eliminates drift in the z-direction, during each

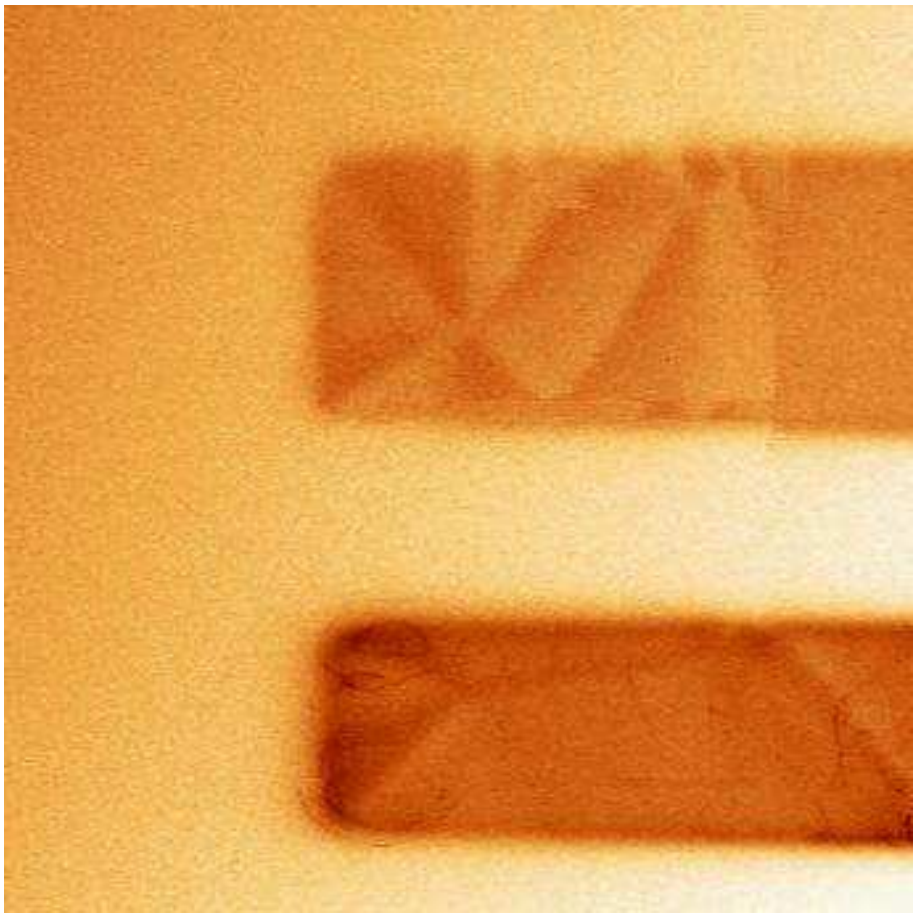

Figure B.2: *One of the last measurements at the ends of 2 2 × 20 μm elements. This image represents the phase signal, with a typical tip-sample distance of 30-50 nm and an oscillation amplitude of* $\sim 10nm$.

line the drift is compensated. The disadvantage is that if there is a lot of non-magnetic material on the surface, the tip will be lifted there as well. This returns in the magnetic image, when the tip is lifted over a non-magnetic feature, the magnetic signal of the underlying magnetic material becomes weaker and you will clearly see those non-magnetic features in the magnetic images, especially if a blunt tip is used. A blunt tip will image itself on any topographic feature, causing tip sample convolution, for example, see figure B.3. Besides surface effects this technique has another major disadvantage; during each scan line the topography is measured using tapping mode, which means the tip has to be in direct contact at the time it hits the surface. The stray fields of the tip can easily change the magnetization of the sample during

the measurement[18, 19]. Many groups have used this technique because it's very easy to use, it's part of the default software package that comes with this type of AFM and there is no drift in the MFM image.

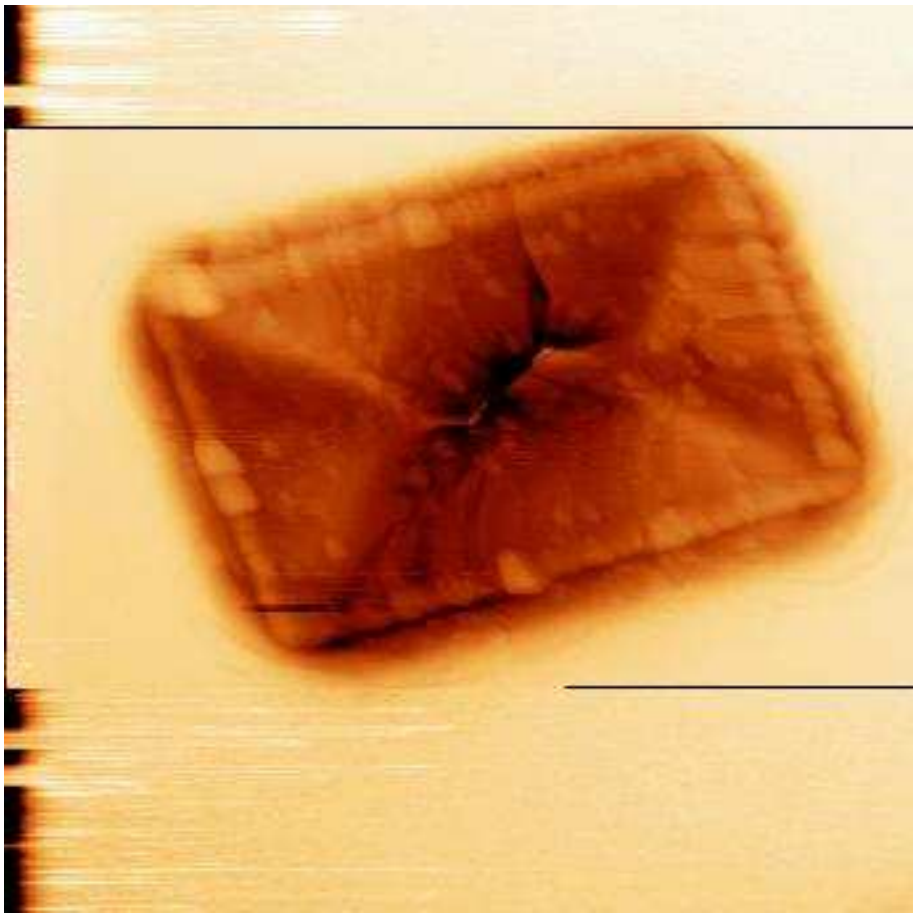

Figure B.3: *An MFM measurement using lift mode. Surface effects are clearly visible in the magnetic image.*

Bibliography

[1] R. D. Gomez, T. V. Luu, A. O. Pak, I. D. Mayegoyz, K. J. Kirk, J. N. Chapman, "Domain wall motion in micron-sized permalloy elements", Journal of applied physics, volume 85, page 4598

[2] M. Barthelmess, C. Pels, A. Thieme, G. Meier, "Stray fields of domains in permalloy microstructures - Measurements and simulations", Journal of Applied Physics, volume 95, page 5641

[3] H. J. Mamin, D. Rugar, J. E. Stern, R. E. Fontana, Jr., P. Kasiraj, "Magnetic force microscopy on thin permalloy films", Appl. Phys. Lett. 55, page 318

[4] Yun-Sok Shin, Hu-Jong Lee, Jinho Kin, Jewook Park, Kookrin Char, "Magnetic Domain Configuration in Cobalt and Permalloy Micro-Structures", Journal of the Korean Phys. Soc., Vol 44, page 904-907

[5] T. Shinjo, T. Okuno, R. Hassdorf, K. Shigeto, T. Ono, "Magnetic Vortex Core Observation in Circular Dots of Permalloy", Science VOL 289, page 930

[6] M. Schneider, H. Hoffman, J. Zweck, "Magnetic switching of single vortex permalloy elements", Appl. Phys. Lett., volume 79, number 19, page 3113

[7] Xiaobin Zhu, P. Grütter, V. Metlushko, B. Ilic, "Magnetic force microscopy study of electron-beam-oatterened soft permalloy particles: Technique and magnetization behavior", Physical review B 66, 024423 (year 2002)

[8] Jong-Ching Wu, Ying-Wen Huang and Te-ho Wu, "Magnetization Reversal in Patterned Single Domain Elements", Jpn. J. Appl Phys. Vol. 38 (year 1999) pp. 6711-6712

[9] Mei-Feng Lai, Zung-Hang Wei, Ching-Ray Chang, J. C. Wu, W.Z. Hsieh, Nickolai A. Usov, Jun-Yang Lai, Y. D. Yao, "Magnetization patterns of permalloy square frames", Journal of Applied Physics, volume 93, page 7426

[10] Kenji Machida, Tomoyuki Tezuka, Takahiro Yamamoto, Takayuki Ishibashi, Yoshitaka Morishita, Akinori Koumitu , Katsuaki Sato, "Magnetic structure of cross-shaped permalloy arrays embedded in silicon wafers.", J. Magn and Magn Mater 290-291, page 779-782

[11] A. Hirohata, C. C. Yao, H. T. Leung, Y. B. Xu, C. M. Guertler, J. A. C. Bland, "Magnetic Domain Studies of Permalloy Wire-Based Structures with Junctions", IEEE Transactions on Magnetics, vol. 36, no. 5, page 3068

[12] Robert C. O'Handley, "Modern Magnetic Materials Principles and Applications" ISBN 0-471-15566-7, John Wiley & Sons, Inc

[13] O.W.B.Benningshof, "Geen goed verslag zonder Fermi bol.", unpublished

[14] T. Trunk, M. Redjdal, A. Kákay, M. F. Ruane, F. B. Humphrey, "Domain wall structure in Permalloy films with decreasing thickness at the Bloch to Neél transition", Journal of applied physics, volume 89, page 7606

[15] Konstantin L. Metlov, "A simple analytical description for the cross-tie domain wall structure.", unpublished

[16] http://www.physics.leidenuniv.nl/sections/cm/ip/welcome.htm

[17] Vasile M J and Mogab C J, "Chemically assisted sputter etching of permalloy using CO or Cl", year 1986, J. Vac. Sci. Technol. A vol 4 page 1841

[18] N. I. Polushkin, B. A. Gribkov, V. L. Mironov, A. M. Alexeev, A. F. Popkov, J. Wittborn, K. V. Rao, "SPM study of patterned magnetic nanostructures for high-density data storage", SPM-2003, Proceedings. Nizhni Novgorod, March 2-5. 2003. P. 51

[19] A.G. Temiryazev, "MFM study of soft magnetic samples" SPM-2003, Proceedings. Nizhni Novgorod, March 2-5. year 2003. P. 161